Biochimica et Biophysica Acta 1848 (2015) 984–994

Contents lists available at ScienceDirect

Biochimica et Biophysica Acta

journal homepage: www.elsevier.com/locate/bbamem

Comparative study of interactions of aliskiren and AT_1 receptor antagonists with lipid bilayers

A. Sadeghpour [a], M. Rappolt [a,*], D. Ntountaniotis [b], P. Chatzigeorgiou [b], K. Viras [b], G. Megariotis [c], M.G. Papadopoulos [c], E. Siapi [c], G. Mali [d], T. Mavromoustakos [b,**]

[a] School of Food Science & Nutrition, University of Leeds, Leeds LS2 9JT, UK
[b] Chemistry Department of National Kapodistrian University, Zografou, Athens 15784, Greece
[c] National Hellenic Research Foundation, Institute of Biology, Medicinal Chemistry& Biotechnology, Vas. Constantinou 48, 11635 Athens, Greece
[d] Laboratory for Inorganic Chemistry and Technology, National Institute of Chemistry, Hajdrihova 19, SI-1001 Ljubljana, Slovenia

ARTICLE INFO

Article history:
Received 15 July 2014
Received in revised form 29 November 2014
Accepted 3 December 2014
Available online 19 December 2014

Keywords:
Aliskiren
Renin
PRR
DPPC bilayer

ABSTRACT

The renin–angiotensin–aldosterone system (RAAS) plays a key role in the regulation of blood pressure. Renin is the rate limiting enzyme of the RAAS and aliskiren is a highly potent and selective inhibitor of the human renin. Renin is known to be active both in the circulating blood stream as well as locally, when bound to the (pro)-renin receptor ((P)RR). In this study we have investigated a possible mechanism of action of aliskiren, in which its accumulation in the plasma membrane is considered as an essential step for effective inhibition. Aliskiren's interactions with model membranes (cholesterol rich and poor) have been investigated by applying different complementary techniques: differential scanning calorimetry (DSC), Raman spectroscopy, magic angle spinning (MAS) nuclear magnetic resonance (NMR) spectroscopy and small- and wide-angle X-ray scattering (SAXS and WAXS). In addition, in silico molecular dynamics (MD) calculations were applied for further confirmation of the experimental data. Aliskiren's thermal effects on the pre- and main transition of dipalmitoyl-phosphatidylcholine (DPPC) membranes as well as its topographical position in the bilayer show striking similarities to those of angiotensin II type 1 receptor (AT_1R) antagonists. Moreover, at higher cholesterol concentrations aliskiren gets expelled from the membrane just as it has been recently demonstrated for the angiotensin receptor blocker (ARB) losartan. Thus, we propose that both the AT_1R and the (P)RR-bound renin active sites can be efficiently blocked by membrane-bound ARBs and aliskiren when cholesterol rich membrane rafts/caveolae are formed in the vicinity of the receptors.

1. Introduction

Hypertension is a risk factor associated with cardiovascular diseases, and the first leading cause of death in economically developed countries. For this reason, medicinal chemists aim to synthesize more effective and novel drugs, which can regulate the blood pressure with longer duration of action and fewer side effects. The most important system which interferes with the regulation of pressure is the renin–angiotensin–aldosterone system (RAAS) [1,2]. RAAS activation is stimulated by a drop in blood pressure, loss of blood volume or reduction in plasma sodium concentration. These signals trigger the release of renin, a highly specific and selective aspartic protease, which cleaves angiotensinogen (Aog) to produce the inactive decapeptide angiotensin I (AngI). AngI is next converted by angiotensin-converting enzyme (ACE) to the active peptide angiotensin II (AngII), which causes vasoconstriction when it binds to the angiotensin subtype 1 receptor (AT_1R) or stimulates the secretion of the hormone aldosterone. Since the rate-limiting step in this cascade is determined by renin to produce AngI, inhibition of this step is an effective therapeutic target against hypertension [3].

For many years, we are studying the interactions of AT_1R antagonist molecules or angiotensin receptor blockers (ARB) that prevent AngII to exert its detrimental effects on AT_1 receptor, with the lipid bilayers and their receptor active site in order to comprehend their molecular basis of action. ARBs are hypothesized to act on the AT_1R by a two-step process [4]. In the first step the drug is incorporated into the membrane, and in the second step it diffuses to the receptor site, where it binds to the active site of the AT_1R [5–7].

For renin, the situation is to some extent different [8]. Renin circulates in the blood plasma, and thus a direct inhibition of renin in the systemic system by aliskiren is possible. However, renin binds with a high affinity to the (pro)-renin receptor ((P)RR) [9–11], and subsequent studies have shown that (P)RR-bound renin has a fourfold higher catalytic activity [12]. Thus a second, local mechanism of action of aliskiren is also possible (Fig. 1A). Due to its high lipophilicity (log P octanol/water = 2.45 at pH 7.4 [13]) aliskiren is expected to accumulate as efficiently in lipid

* Corresponding author. Tel.: +44 113 3431931.
** Corresponding author. Tel.: +30 2107274475.
E-mail addresses: m.rappolt@leeds.ac.uk (M. Rappolt), tmavrom@chem.uoa.gr (T. Mavromoustakos).

http://dx.doi.org/10.1016/j.bbamem.2014.12.004
0005-2736/

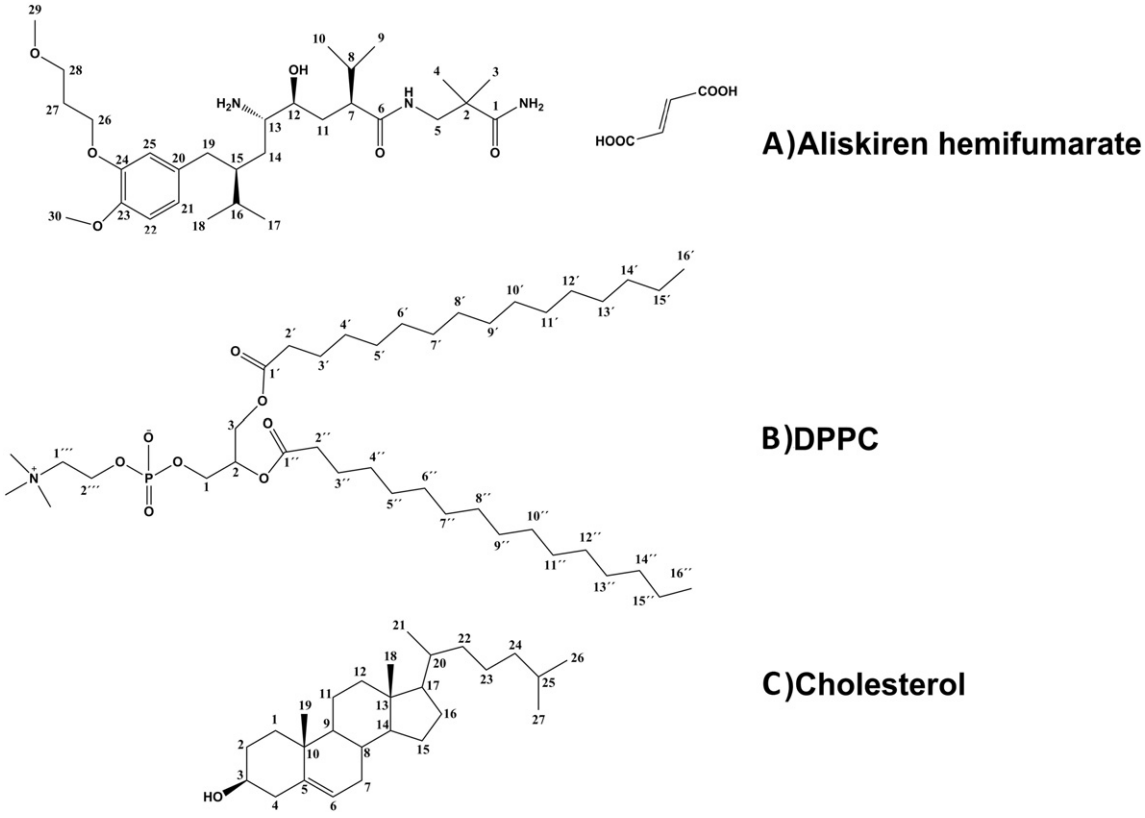

Fig. 1. Molecular structures of aliskiren (A), DPPC (B), and cholesterol (C).

bilayers as the comprehensively studied ARBs [14–17]. In this study we therefore investigate the binding of aliskiren to different lipid bilayer models (both, cholesterol poor and rich) and put the results in context with the extensively studied AT_1R antagonists for an improved understanding of the local interactions of aliskiren with (P)RR bound renin.

Cell plasma membranes have a complex architecture hosting various kinds of protein receptors which for the assembly of signalling molecules are believed to get organized in cholesterol rich micro-domains (rafts). The most abundant lipid species in the lipid matrix of the vascular smooth muscle cells [18] and sarcolemma cardiac membranes [19] are phosphatidylcholines (PCs). The most frequently found among them are PCs with oleic and linoleic chains, and further dipalmitoylphosphatidylcholine (DPPC). Hydrated DPPC bilayer models (poor and rich in cholesterol) have been therefore applied to investigate aliskiren-bilayer interactions (Fig. 1B and C) as they comprise very convenient mesomorphic states (gel, gel/fluid and fluid) and their thermal as well as dynamic properties have been studied thoroughly [20].

In this context, we have initiated a new research activity that aims to compare the membrane effects of aliskiren with those of AT_1R antagonists, since both classes of molecules act in the same system and have been used synergistically to affect the biomembrane and increase their therapeutic index [21,22].

To undertake this task, we have studied interactions between drug and lipid bilayers using differential scanning calorimetry, Raman spectroscopy, solid-state magic angle spinning (MAS) NMR spectroscopy and small- and wide angle X-ray scattering. In addition, we have complemented our studies using in silico MD simulations.

2. Materials and methods

2.1. Materials

Dipalmitoyl-phosphatidylcholine and cholesterol were purchased from Avanti Polar Lipids (Birmingham, AL), and used without further purification. The salt form of aliskiren (aliskiren-hemifumarate) was kindly supplied by Novartis (Basel).

2.2. Differential scanning calorimetry

For DSC experiments about 7 mg 50% (w/w) liposomal dispersions were used. The aliskiren concentrations were 5, 10, 15 and 20 mol.% and the cholesterol concentration varied from 12 to 15 mol.%. All samples were scanned from 25 to 50 °C at least three times until identical thermal scans were obtained using a scanning rate of 2.5 °C/min. Further details of the sample preparation, set-up and data analysis can be found in our previous publications [14,16,17].

2.3. Raman spectroscopy

The samples' preparation for the Raman measurements was identical to that for DSC. Raman spectra were recorded with a Perkin-Elmer GX Fourier Transform spectrometer (Shelton, CT). Raman spectra of the examined samples were obtained in the frequency region of 3500–400 cm^{-1} and in the temperature range 25 to 50 °C. Further experimental details can be found in our previous publications [14–17].

2.4. MAS NMR

Sample preparation for solid-state NMR was identical to that for DSC. The samples (20 μL) were transferred to 3.2 mm zirconia rotors. ^{13}C MAS and ^{13}C cross polarization (CP)MAS NMR spectra were obtained at 150.80 MHz with a 600 MHz Varian spectrometer (Palo Alto, CA). The spinning rate used was 5 kHz. The experimental temperatures were 25, 35, and 45 °C for CP/MAS experiments and 45 °C for the MAS measurement. Chemical shifts were reported relative to 13C resonance of tetramethylsilane. For both measurements the number of scans were 400 and the relaxation delay was 5 s. Polarization transfer in the CP/MAS measurements was achieved with RAMP cross-polarization [23]

(ramp on the proton channel) with a contact time of 5 ms. High-power continuous-wave hetero-nuclear proton decoupling was applied during acquisition.

2.5. X-ray scattering

The samples for the X-ray scattering experiments were prepared in a similar way as for DSC measurements. Time resolved simultaneous small- and wide-angle X-ray scattering (SAXS and WAXS) experiments were carried out at the Austrian SAXS beamline at ELETTRA, Trieste [24,25]. The experimental details of the set-up and sample environment are described in previous works [14–17]. The samples were heated from 20 to 60 °C and back to 20 °C with a scan rate of 1 °C/min. Static exposures were taken before and after each scan and their duration was 15 s.

In the time resolved X-ray scattering experiments, the *d*-spacings of the gel and fluid phases were derived by standard procedures [26,27]. In particular cases, the SAXS patterns were analysed globally applying the modified Caillé theory [28–30]. This global fitting technique is described in details elsewhere [31–34]. The headgroup-to-headgroup thickness, d_{HH}, and the bending fluctuation (Caillé parameter),

$$\eta = \frac{\pi k_B T}{2d^2\sqrt{(K_C B)}} \tag{1}$$

were directly obtained from the fits (K_C, denotes the membrane bending rigidity, B the compression bulk modulus, k_B the Boltzmann constant, T the temperature and d the lattice spacing).

2.6. Molecular dynamics

Aliskiren topology files were produced by PRODGR server. A bilayer of 128 dimyristoyl-phosphatidylcholine (DMPC) and another with DPPC molecules were simulated with a united atom representation and the topology files were downloaded from the Tieleman Web page [35–37], while 3655 water molecules were described by the Simple Point Charge (SPC) model. Three different concentrations of aliskiren were simulated i.e., 1 (equal to 0.8 mol.%), 5 (4 mol.%) and 11 (8 mol.%) molecules, which are all placed initially in the aqueous phase. Each system was energy-minimized using the steepest descent method and next the molecular dynamics (MD) simulations were commenced for 250 ns. All simulations were performed with the MD package GROMACS 4.5.1 [36,38–40]. Equations of motion were integrated with a 2 fs time step and all bonds were constrained to their equilibrium length with the LINCS algorithm. The temperature was kept constant at 325 K using the Berendsen thermostat with a 0.1 ps coupling time constant, while the Berendsen barostat was employed for the semi-isotropic pressure coupling of the bilayer at 1 bar. For the non-bonded interactions of the system, a cut-off radius of 10 Å was applied with pressure and energy correction terms due to the truncation of the potentials. The PME technique was used for the treatment of long range electrostatics.

Table 1
Representative diagnostic thermal effect values for DPPC and DPPC/cholesterol bilayers without or with aliskiren.

Samples	T_m (°C)	ΔT_m (°C)	ΔH (kcal/mol)
DPPC	41.20 ± 0.1	0.9 ± 0.1	7.33 ± 0.08
DPPC/aliskiren 95:5	40.93 ± 0.1	1.6 ± 0.1	7.86 ± 0.08
DPPC/aliskiren 90:10	39.08 ± 0.1	0.9 ± 0.1	9.46 ± 0.09
DPPC/aliskiren 85:15	38.13 ± 0.1	1.1 ± 0.1	10.04 ± 0.10
DPPC/aliskiren 80:20	38.34 ± 0.1	1.5 ± 0.1	10.45 ± 0.10
DPPC/cholesterol 85:15	40.60 ± 0.1	1.0 ± 0.1	5.12 ± 0.05
[DPPC/cholesterol 85:15]/aliskiren 95:5	37.97 ± 0.1	1.5 ± 0.1	6.47 ± 0.06
[DPPC/cholesterol 85:15]/aliskiren 80:20	36.80 ± 0.1	1.9 ± 0.1	7.33 ± 0.07

The deuterium order parameter (S_{cd}) of the alkyl tails is given by the following equation:

$$-S_{CD} = \frac{2}{3}S_{xx} + \frac{1}{3}S_{yy} \tag{2}$$

in which:

$$S_{ij} = \frac{1}{2}\left\langle 3\cos\theta_i\ \cos\theta_j - \delta_{ij}\right\rangle \tag{3}$$

Details on how the components are computed can be found in other studies [36,38].

3. Results

3.1. Differential scanning calorimetry

The thermal changes of the DPPC and DPPC/cholesterol bilayers in the absence and presence of aliskiren have been analysed in DSC measurements (see Supporting Information, Fig. S1). In Table 1 the quantitative data of the diagnostic parameters (T_m, ΔT_m, and ΔH) are presented. In pure DPPC, both the pre-transition (lamellar gel phase, $L_{\beta'}$ [41] to the ripple phase, $P_{\beta'}$ [42]) as well as the main-transition (formation of the fluid lamellar phase, L_α [43]) are observed. The recorded transition temperatures ($T_{pre} = 37.6 \pm 0.3$, $\Delta T_{pre} = 1.0 \pm 0.3$, $T_m = 41.20 \pm 0.1$, $\Delta T_m = 0.9 \pm 0.1$) and enthalpies ($\Delta H_{pre} = 1 \pm 0.02$, $\Delta H = 7.33 \pm 0.08$) for pure DPPC bilayers are in good agreement with literature values [20].

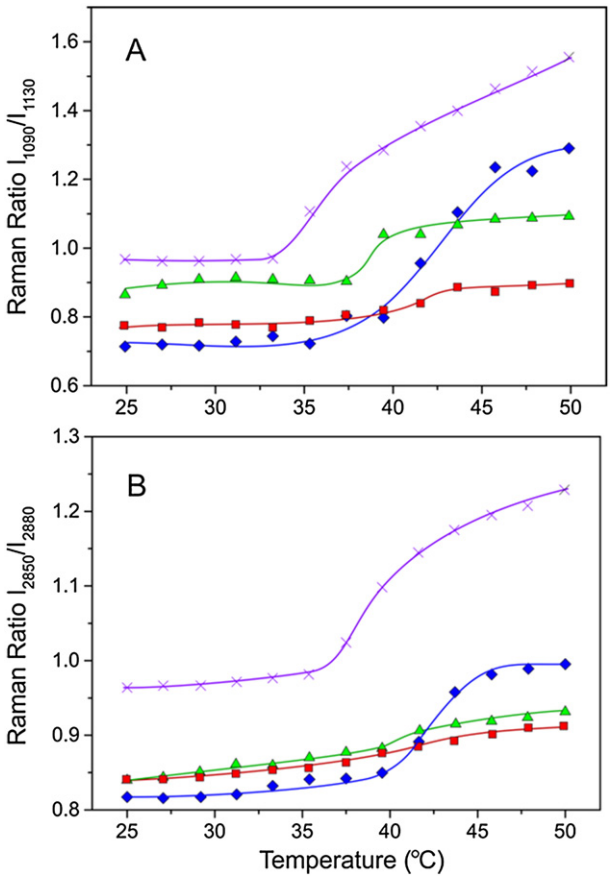

Fig. 2. (A) I_{1090}/I_{1130} vs. temperature plots for pure DPPC (♦), DPPC containing 20 mol.% of aliskiren (■), DPPC containing 15 mol.% cholesterol (▲) and [DPPC/cholesterol (85/15)]/aliskiren (80/20) (X). The same symbolic is used for panel B representing I_{2850}/I_{2880} vs. temperature plots.

Addition of aliskiren at low concentration (5 mol.%) broadens the main phase transition and abolishes the pre-transition without causing significant effect on the phase transition temperature, T_m, and on the enthalpy, ΔH. The use of the higher concentrations of aliskiren (10–20 mol.%), results in a further progressive decrease of T_m and an increase of ΔH. Two concentrations of aliskiren (5 and 20 mol.%) were used to examine its thermal effects on DPPC/cholesterol bilayers. In both cases the pre-transition gets suppressed, while the main phase transition broadens, T_m decreases slightly and ΔH decreases (Table 1).

3.2. Raman spectroscopy

Raman spectra of pure DPPC, DPPC/aliskiren (80/20), DPPC/cholesterol (85/15), and [DPPC/cholesterol (85/15)]/aliskiren (80/20) bilayers were obtained in a temperature range of 25–50 °C. Spectral bands in region from 1000 to 1150 cm^{-1} are related to the hydrocarbon skeletal C–C stretching modes. In particular, the bands at ~1090 cm^{-1} and ~1130 cm^{-1} reflect the C–C stretching modes in *gauche* and *trans* conformations, respectively [16,17,44,45]. The C–H stretching bands at ~2850 cm^{-1} and ~2880 cm^{-1} are due to symmetric and antisymmetric stretching modes in the methylene groups (CH_2) of the alkyl chains, respectively, while the ~2935 cm^{-1} band is correlated to the symmetric C–H stretching mode in the terminal methyl group [45–47]. The two intensity ratios I_{1090}/I_{1130} and I_{2850}/I_{2880} (Fig. 2) reflect the transition behaviour of the different bilayers studied and in particular describe the fluidity of the membranes. How aliskiren influences the order/disorder of the different model membranes is discussed in Section 4.1.

3.3. MAS NMR

To obtain a detailed local information on the incorporation of aliskiren and cholesterol in the DPPC bilayers, we applied high resolution ^{13}C MAS and CP/MAS NMR spectroscopy [48] (Fig. 3). Observed chemical shifts for the carbons of DPPC are summarized in Table 2 for DPPC, DPPC/cholesterol (85/15), DPPC/aliskiren (80/20), and [DPPC/cholesterol (85/15)]/aliskiren (80/20) bilayers (see also Supporting Information Tables S1 and S2). The spectra are presented according to the (i) headgroup, (ii) glycerol backbone, (iii) esterified carbonyl, and (iv) hydrophobic lipid chain regions (for carbon identifiers of DPPC bilayers refer to Fig. 1B).

3.3.1. Head-group region

Minor changes are observed for the four preparations in the headgroup region ($N(CH_3)_3$, C-2‴and C-2‴). The head-group conformational changes from gel to liquid crystalline phase are less pronounced compared to those observed in the hydrophobic lipid chain region (cp. Section 3.3.4). Further also the presence of aliskiren and cholesterol causes only minor chemical shift increases (maximum down field effect of 0.13 ppm). Indeed, chemical shifts of DPPC/aliskiren, DPPC/cholesterol and DPPC/cholesterol and DPPC/aliskiren preparations are alike, indicating that cholesterol and aliskiren are affecting the headgroup region similarly.

3.3.2. Glycerol backbone region

A downfield shift was observed during the phase transition from the gel to liquid crystalline state for the four different membrane models

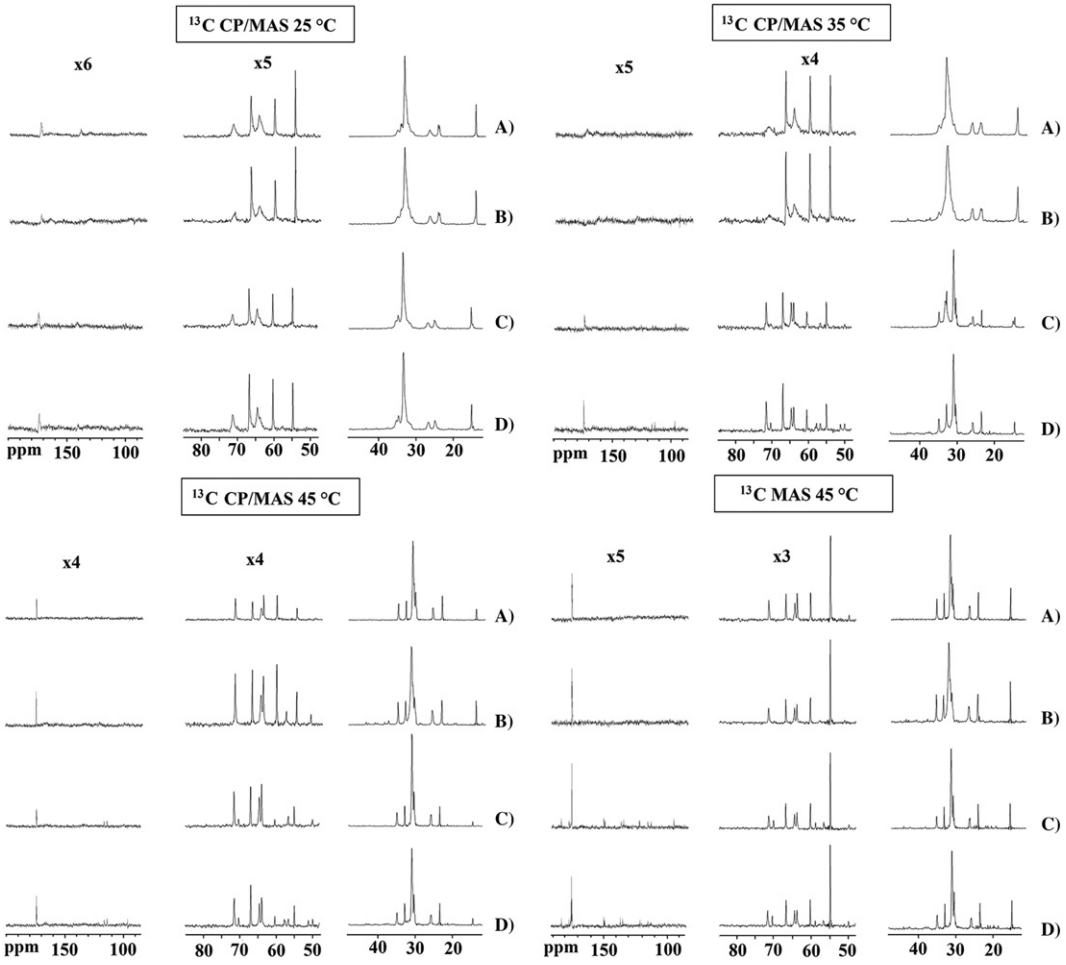

Fig. 3. Observed chemical shifts for the carbons of DPPC in ^{13}C CP/MAS spectra at 25, 35 and 45 °C for (A) DPPC, (B) DPPC/cholesterol (85/15), (C) DPPC/aliskiren (80/20), and (D) [DPPC/cholesterol (85:15)]/aliskiren (80:20) bilayers.

Table 2
Observed chemical shifts for the carbons of DPPC in ^{13}C MAS and CP/MAS spectra in a temperature range of 25–45 °C.

		Glycerol carbons			Carbonyl carbons			Hydrophobic chain region				Headgroup region		
T (°C)	Sample	C-1	C-2	C-3	C-1′, C-1″	C-2′, C-2″	C-3′, C-3″	$(CH_2)'_{10}$, $(CH_2)''_{10}$	C-14′, C-14″	C-15′, C-15″	C-16′, C16″	$N(CH_3)_3$	C-2‴	C-1‴
^{13}C-MAS														
45	DPPC	63.80	71.41	64.41	174.02	34.81	25.86	31.10	32.83	23.41	14.49	54.89	66.82	60.21
45	DPPC/cholesterol (85/15)	63.88	71.45	64.53	174.19 +174.00	34.93	26.04	31.51	33.00	23.54	14.55	54.93	66.84	60.28
45	DPPC/aliskiren (80/20)	63.93	71.53	64.59	174.20	34.91	25.90 25.76	30.92 30.35	32.85	23.47	14.64	54.98	66.95	60.32
45	[DPPC/cholesterol (85/15)]/aliskiren (80/20)	63.92	71.48	64.59	174.20	34.91	25.90 25.75	30.96 30.36	32.85	23.47	14.64	54.95	66.93	60.30
^{13}C CP/MAS														
25	DPPC	–	71.22	64.38	172–174	34.98	26.72	33.25	34.22	24.44 24.17	14.65	54.76	66.63	60.22
25	DPPC/cholesterol (85/15)	–	71.22	64.48	172–174	35.15	26.82	33.26	34.26	24.48 24.15	14.70	54.79	66.66	60.26
25	DPPC/aliskiren (80/20)	63.85	71.29	64.50	173–175	35.16	26.57	33.31 32.19	34.62	24.64 24.90	(15.06) 14.65	54.79	66.76	60.23
25	[DPPC/cholesterol (85/15)]/aliskiren (80/20)	63.83	71.33	64.52	173–175	35.22	26.63	33.32	34.65	24.68 24.91	(15.09) 14.61	54.81	66.74	60.25
35	DPPC	–	71.14	64.38	172–175	35.10	26.37	33.11	–	24.25	14.60	54.79	66.69	60.20
35	DPPC/cholesterol (85/15)	–	71.21	64.47	172–175	35.19	26.46	33.10	–	24.29	14.65	54.92	66.81	60.33
35	DPPC/aliskiren (80/20)	63.95	71.51	64.62	174.21	34.96	25.89	31.06 30.46	33.30 32.93	24.60 23.55	(15.12) 14.71	54.98	66.94	60.34
35	[DPPC/cholesterol (85/15)]/aliskiren (80/20)	63.91	71.44	64.59	174.17	34.91	25.90	31.00 30.42	32.89	23.53	14.66	54.93	66.87	60.31
45	DPPC	63.77	71.37	64.49	174.03	34.81	25.85	31.06	32.79	23.39	14.49	54.86	66.81	60.19
45	DPPC/cholesterol (85/15)	63.86	71.43	64.55	174.17	34.93	26.02	31.43	32.97	23.53	14.55	54.93	66.85	60.27
45	DPPC/aliskiren (80/20)	63.93	71.53	64.56	174.16	34.93	25.87 25.76	30.89 30.32	32.82	23.48	14.63	55.00	66.97	60.32
45	[DPPC/cholesterol (85/15)]/aliskiren (80/20)	63.93	71.48	64.58	174.18	34.92	25.88 25.76	30.92 30.34	32.83	23.46	14.63	54.97	66.95	60.31

ranging between 0.11 and 0.24 ppm indicating their conformational stability in this bilayer region (C-1, C-2, C-3). Cholesterol causes downfield changes up to 0.1 ppm, when comparing DPPC/cholesterol and DPPC bilayers at the same temperatures. When the DPPC/aliskiren and DPPC bilayers are compared, higher downfield shifts reaching 0.37 ppm are observed. DPPC bilayers containing both aliskiren and cholesterol show similar chemical shifts with those containing DPPC and aliskiren.

3.3.3. Carbonyl region

The resolution for C-1′ in the four preparations was not sufficient to follow the chemical shift changes during the phase transition. For C-2′ a biphasic effect was observed, i.e., a downfield effect in the ripple phase and an upfield effect in the fluid lamellar phase. For C-3′ a progressive upfield effect (decrease of chemical shift) was eminent as the temperature increases reaching 0.7 ppm in the L_α phase, indicating that this carbon in the carbonyl region behaves similarly to all other carbons at the hydrophobic region. Similar effects were observed for the DPPC/cholesterol sample. In DPPC/aliskiren bilayers a progressive upfield effect (<1 ppm) was observed for C-3′ and C-2 . Similar upfield effect (<1 ppm) was also obtained in the case that both aliskiren and cholesterol are incorporated in the DPPC bilayers, i.e., DPPC/aliskiren and DPPC/cholesterol/aliskiren bilayers showed similar chemical shifts.

3.3.4. Hydrophobic lipid chain region

The chemical shifts decrease when DPPC bilayers undergo the transition from the lamellar gel phase $L_{ß'}$ (25 °C) towards the ripple phase $P_{ß'}$ (35 °C) and lamellar liquid crystalline phase L_α (45 °C). This is due to the strong *trans–gauche* isomerization effects observed especially in the turnover to the L_α phase. Upfield effect of the carbons which constitute the hydrophobic region was also observed in DPPC/cholesterol and DPPC/aliskiren bilayer samples. The most pronounced upfield effect was with $(CH_2)'_{10}$ carbons reaching almost 3 ppm while with C-16 , C-15 and C-14 the effect was ranging between 0.02 and 1.40 ppm.

3.4. X-ray scattering

In Fig. 4 an overview of the time-resolved SAXS/WAXS experiments is presented. In the contour plots high scattering intensities are colour-coded with red and orange, while lower scattering intensities are given in green and blue.

The structural changes in pure DPPC bilayers [49] are exemplified in Fig. 4A. At ambient temperatures the lamellar gel phase ($L_{\beta'}$) is observed. The chains are packed in an orthogonal lattice [44,45] and tilted with respect to the bilayer plane about 32° [50]. Thereafter, the stable ripple phase ($P_{\beta'}$) forms, followed by the lamellar fluid phase (L_α). Note, that the transition is not reversible, but in cooling direction two ripple phases form: the stable and the so-called metastable ripple phase ($P_{\beta'}$ and $P_{\beta'\ mtstbl}$) [51]. The interaction of 10 mol.% cholesterol with phosphatidylcholine bilayers is presented in Fig. 4B. Both in the gel and the fluid phase regime cholesterol induces in part a liquid ordered (lo) phase, where the lipids are free to laterally diffuse, but at the same time exhibit a certain chain order [52–54].

As can be seen in the SAXS patterns in Fig. 4C, aliskiren provokes in the gel phase the onset of an unbinding of the bilayers. The first order diffraction peak is centred at $s = 0.007$ Å^{-1}, which corresponds to a *d*-spacing of about 140 Å. This means that the bilayers are about 100 Å apart. In other words the multilamellar vesicles (MLVs) are highly swollen with water. In the fluid phase regime the unbinding of bilayer membranes is complete, i.e., the bilayers are spatially uncorrelated.

In contrast to the effect of aliskiren alone, the incorporation of aliskiren together with cholesterol in the DPPC bilayers reduces the *d*-spacing drastically from 140 to 72 Å (Figs. 4D and 5B). The *d*-spacing of 72 Å in the lamellar gel-phase can actually be explained by a loss of

chain tilt in the lamellar gel phase. This is supported by a determined bilayer thickness, d_{HH}, of 50 Å deduced from the electron density profile of the bilayer (Supporting Information Figs. S2–S3 and Table S3; note that a complete loss of chain tilt would result in a *d*-spacing of about 72 Å [48]). However, in the fluid phase a coexistence of highly swollen MLVs (maximum *d*-spacing is 102 Å, Fig. 5B) together with a high fraction of spatially uncorrelated bilayers is observed.

The temperature dependent lipid chain packing of the four different studied samples is presented in Fig. 6. The lipid chain packing gives a relatively good indication for T_m. The melting point for pure DPPC bilayers is determined with the WAXS recordings to be at 43 °C, while with decreasing lipid concentration the melting point is observed at 42, 40 and 38 °C, respectively. This is readily understood, since an increasing concentration of impurities in the form of cholesterol and/or aliskiren reduces the overall van der Waals energy. Another effect can be observed in the packing density of the lipid chains in the gel phase. For instance, at 37 °C the first order diffraction peak indicates an averaged nearest neighbour distance of the lipid chains of 4.27 Å for DPPC bilayers (area per chain 21.0 Å^2). Aliskiren alone has a condensing effect (d = 4.20 Å at 37 °C), whereas 10 mol.% cholesterol causes an overall looser chain packing in the gel phase: the *d*-spacing is about 4.31 Å in both the DPPC/cholesterol as well as the DPPC/aliskiren/cholesterol bilayer systems. This is understood, since cholesterol above a certain threshold (typically > 5 mol.%) induces in part the lo-phase, in which the apparent area per lipid is enhanced.

3.5. Molecular dynamics

The effect of aliskiren molecules on DMPC and DPPC model membranes was examined with MD simulations at three different concentrations of the drug, i.e., for one, five and eleven molecules per 128 lipids (0.8, 4 and 9 mol.%). The density profiles of all individual components in the system along the axis orthogonal to the bilayer (z-axis) are depicted in Fig. 7. Obviously aliskiren molecules diffuse into the interior of the bilayer even though their initial positions in the simulations were given in the aqueous phase.

Another important property of a lipid-bilayer system is the area per lipid which may be estimated by a variety of experimental techniques (e.g., NMR, X-ray diffraction). Most of the experimental values lie between 61 and 67 Å^2/lipid indicating that the membrane is in the liquid crystalline phase. Similar results are obtained by our simulations as listed in Table S4. Moreover, there is an increase for the area per lipid as more aliskiren molecules are added. Focusing on the headgroup of lipids, the angle between the vector connecting P and N atoms and the z-axis is important. The presence of aliskiren does not affect the values of the angle as seen in Table S4. Furthermore, the radial distribution function (RDF) between water oxygen and phosphate oxygen was computed to evaluate the influence of the drug on the interface between DPPC and aqueous phase. No significant effect was observed by the aliskiren on the RDF (Fig. 7C).

The order parameters of DMPC bilayers are presented in Fig. 8A and are in agreement with reported data using 2H solid state NMR spectroscopy [55,56]. They were averaged over the two alkyl tails of DMPC and clearly show upward shifting as the number of drug molecules increase. Fig. 8B instead represents the change of order parameter as the number of loaded aliskiren molecules varies from 1 to 11. Accordingly, the highest change in the order parameter occurs in carbon numbers of 6 to 9 (highlighted region in Fig. 10B). The results suggest that the aliskiren molecules mainly sit at the middle of the hydrophobic tails of the lipid. Note that both aliskiren simulation sets on DMPC and DPPC

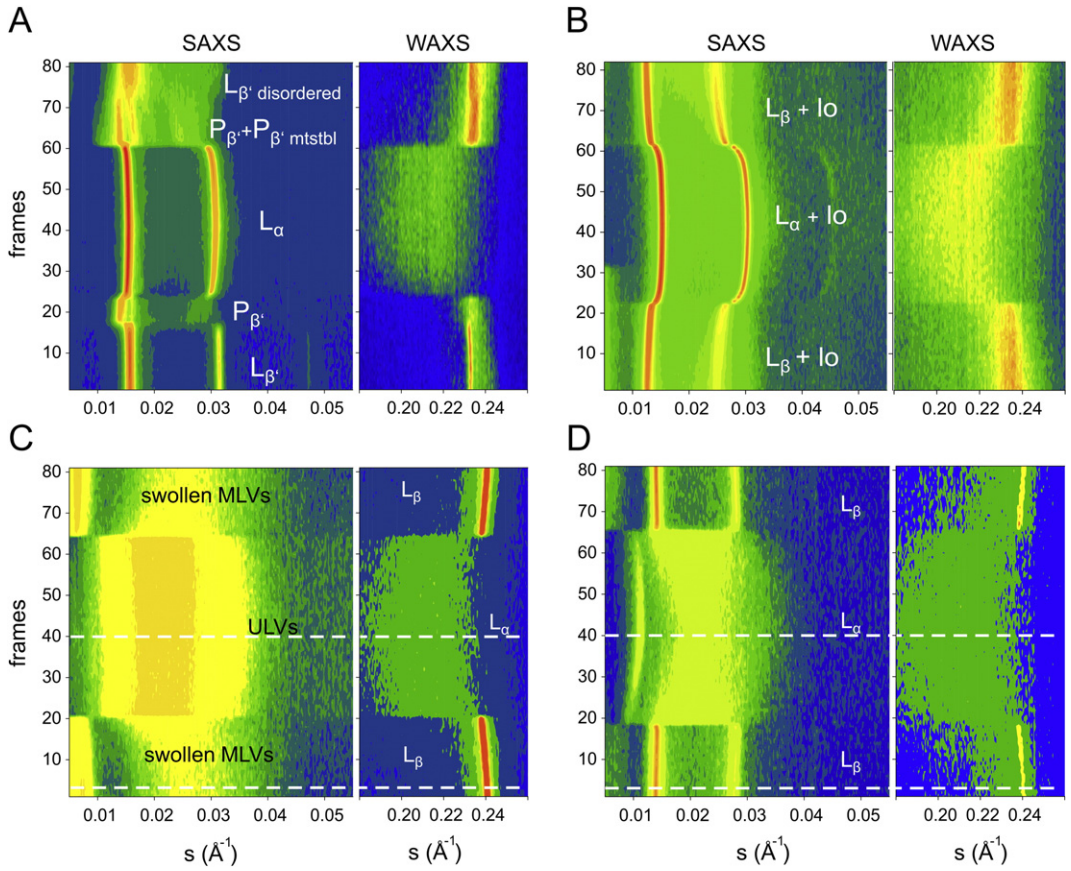

Fig. 4. Temperature scan of multilamellar vesicles of (A) DPPC from 20 to 60 °C and back to 20 °C with 1 °C/min. Note that at frame numbers 1 and 80 the sample temperature was 20 °C and the maximum temperature was reached at frame 40. For the phase assignments refer to the main text. (B) DPPC/cholesterol (90/10), (C) DPPC/aliskiren (80/20) and (D) [DPPC/cholesterol (90/10)]/aliskiren (80/20).

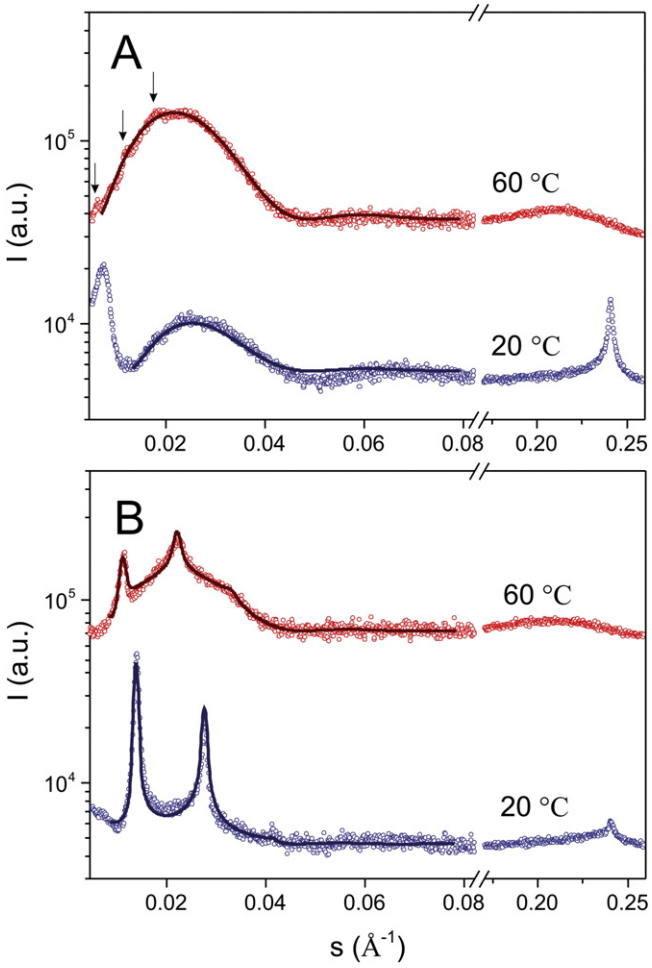

Fig. 5. The scattering profiles of A) DPPC/aliskiren and B) DPPC/cholesterol/aliskiren at two different temperatures. The profiles corresponding to the dashed lines are indicated in Fig. 4C and D. The solid lines are the global fits of the SAXS data (see Section 2.4). Additionally, the electron density map of the DPPC/cholesterol/aliskiren bilayer at 20 °C has been determined (see Supporting Information Figs. S2–S3 and Table S3).

bilayers display very similar results, i.e., demonstrating that a small change in chain length does not have a significant influence on the incorporation of aliskiren.

4. Discussion

4.1. Bilayer interactions with aliskiren

According to the differential scanning calorimetric data, aliskiren at 5 mol.% broadens significantly the $\Delta T_{1/2}$ showing that this low concentration acts as an "impurity". At higher concentrations, aliskiren progressively lowers the phase transition temperature and increases ΔH, while it affects less $\Delta T_{1/2}$. Similar increases in the ΔH, at high concentrations (>10 mol.%) have also been observed for the AT_1R antagonists losartan, irbesartan, valsartan and candesartan cilexetil, but not for candesartan. In addition, this progressive broadening of the phase transition and abolishment of the pretransition was more eminent to losartan, valsartan and candesartan cilexetil, but not for candesartan [16,17,57]. This increase of ΔH, has been interpreted in our previous publications to be associated with partial interdigitation of the lipid chains in the gel phase. In fact the SAXS results of DPPC/aliskiren bilayers at 20 °C support this probable cause: the membrane thickness, d_{HH}, decreases from 44 Å for pure DPPC bilayers to about 31 Å in the presence of aliskiren (Fig. 9A).

Intramolecular *trans–gauche* conformational changes within the hydrocarbon chain region can be monitored directly by the intensity ratio I_{1090}/I_{1130} in Raman spectroscopy. This intensity ratio at this peak height allows the direct comparison of the bilayer disorder–order transitions between liposome preparations without or with drug incorporation. In Fig. 2A the changes in Raman ratio of I_{1090}/I_{1130} are presented. The transition temperatures are well consistent with the results from the calorimetric measurements. DPPC bilayers show a strong increase in Raman ratio across the gel to liquid crystalline phase ($\Delta I = 0.58$), which means rising up of about 80%. Incorporation of aliskiren into these bilayers induces higher disorder in gel phase and less disorder in fluid phase, when compared to the pure DPPC bilayers system. Note, the increase of this Raman ratio across the gel to liquid phase is only about 22% (from 0.88 to 1.1). The intensity ratio I_{2850}/I_{2880} (Fig. 2B) describes the main change occurring in the hydrocarbon-chain region of the lipids and corresponds to intermolecular interactions among aliphatic chains [58]. It is sensitive to subtle changes in conformational order from rotations, kinks, twists and bends of the lipid chains [59]. Alike to the ratio I_{1090}/I_{1130} the presence of aliskiren causes significant increase in the I_{2850}/I_{2880} meaning that drug loading causes disorder in the lipid bilayers in the gel phase. Thus, consistently the two ratios show that aliskiren causes fluidization of the lipid bilayers. However, the Raman spectroscopy results show distinct differences between the effects of aliskiren in DPPC bilayers as compared to AT_1R antagonists. Aliskiren increases the *trans–gauche* ratio to a lesser extent than ARBs (e.g., olmesartan increases that ratio with significantly stronger extent, i.e. from 0.9 to 1.7 [16]).

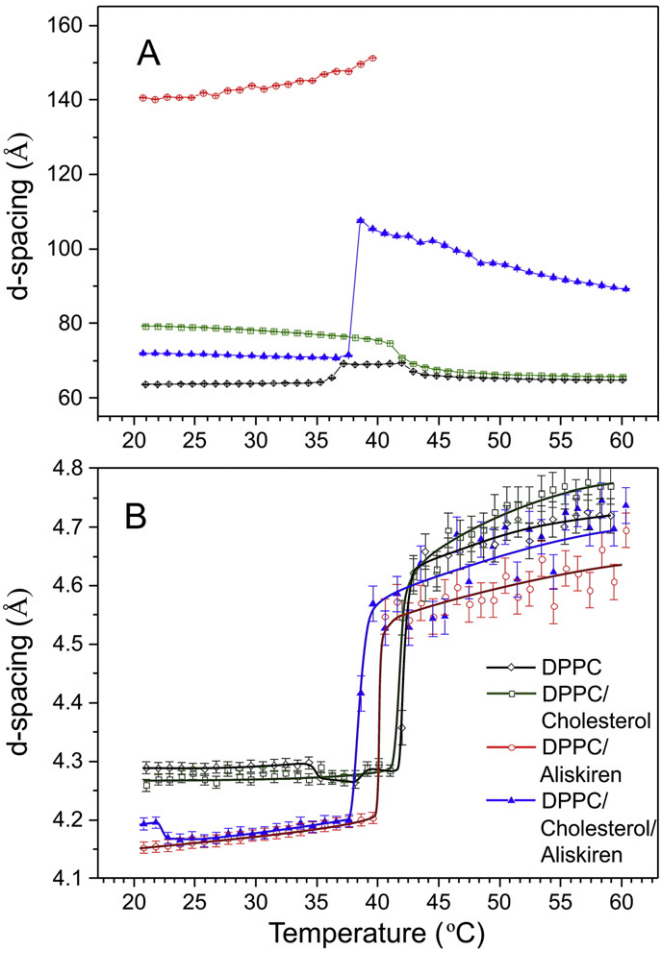

Fig. 6. Lattice spacing of the first order diffraction peaks of DPPC (black), DPPC/cholesterol (90/10) (green), DPPC/aliskiren (80/20) (red), and of [DPPC/cholesterol (90/10)]/aliskiren (80/20) (blue) bilayers. The WAXS analysis displays the nearest neighbour chain to chain distances derived from the first order diffraction peaks in the gel phase and rough distances are determined from the position of the diffuse scattering maximum in the fluid phase.

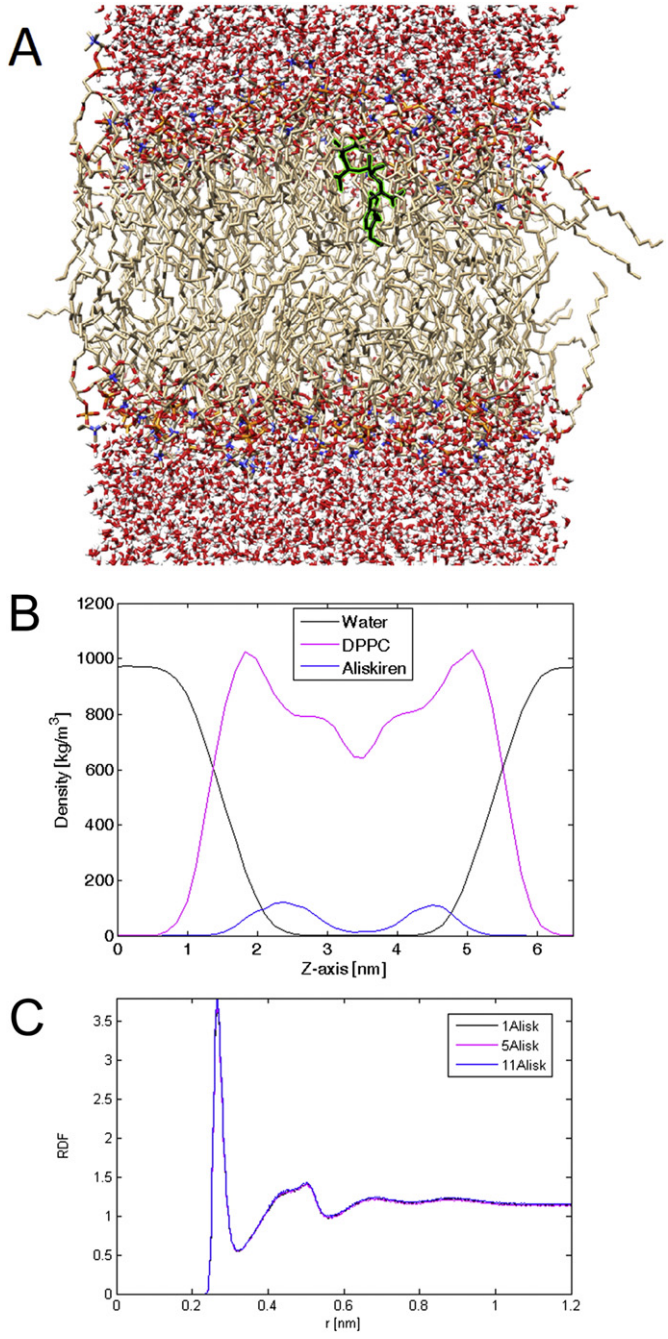

Fig. 7. Molecular dynamics simulations of aliskiren DPPC membrane interactions. A) Snapshot of aliskiren in the DPPC bilayer (128 lipids, 3655 water molecules). B) Density profiles along the z-axis of the DPPC bilayer for the system with 11 aliskiren molecules. C) Phosphate oxygen to water oxygen radial distribution function for the three different concentrations of aliskiren molecules.

^{13}C MAS spectra were especially used to detect the aromatic region, while the ^{13}C CP/MAS spectra of this region were not as eminent (Fig. 2). At 35 °C, the findings reveal a narrowing of the peaks in aliskiren loaded membranes as compared to the DPPC bilayers alone, indicating a change in fluidity of the lipid bilayers in the ripple phase regime ($P_{\beta'}$ phase). When AT_1R antagonists or aliskiren is present, this phase gets suppressed, which is in agreement with DSC results. However, there is an exception to the rule, the ARB olmesartan does not cause an abolishment of the pre-transition and no narrowing of the peaks at 35 °C was observed indicating the complex motions of the lipids existing in the P_{β} phase.

The interdigitation effect induced by aliskiren can be further corroborated by the X-ray diffraction data. As presented in the results section (Fig. 5A), the head–head distance (d_{HH}) is about 31.4 Å in the presence of aliskiren. This value is far smaller compared to the d_{HH} value of 44.2 Å for pure DPPC bilayers [43]. Accordingly, one may conclude that the chain tilt loss is accompanied by the interdigitation of the hydrophobic layer by about 13 Å (Fig. 9A). Consequently, one expects the area per lipid to increase, and this is exactly what the MD simulations data confirm as the aliskiren concentration increases (Table S4).

Another apparent effect of aliskiren is the induction of strong water swelling of the MLVs, i.e. the bilayers separation increases from 19 to 100 Å at 20 °C and from 28 to 130 Å at 60 °C (Fig. 9). Note also, that actually only a small fraction of the membranes remain spatially correlated in the fluid phase, while the biggest fraction of bilayers completely unbinds (cp. Fig. 5). In contrast in the gel phase the main fraction of the sample remains ordered. Here the swelling can be explained by electrostatic repulsion induced by the positively charged aliskiren molecules at pH 7 (aliskiren has only one pK_a value of 15.9, and hence has strong basic proprieties [60]; note membrane undulations usually play a minor role in the gel phase). In the fluid phase instead both electrostatic repulsion as well as the onset of membrane undulations will contribute to the increase in bilayer separation. This means that above the melting point the onset of Helfrich-undulations of the membranes delivers one part of the explanation. However, the electrostatic repulsion force is expected to diminish above T_m. As long as the partition coefficient of aliskiren can be assumed to be temperature independent, then this force diminishes in the fluid phase, simply because the surface charge density decreases (note, the area per lipid increases above T_m). Thus, both increased membrane undulations and a higher partition

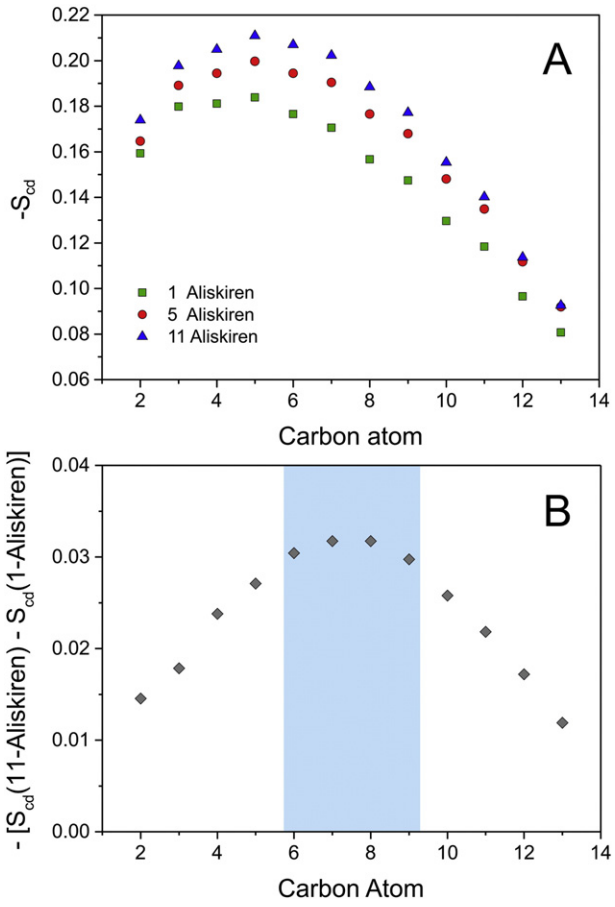

Fig. 8. A) Deuterated order parameters for the alkyl tails of DMPC in presence of aliskiren molecules as obtained from the MD simulations. B) Difference in the order parameter between the alkyl chains of highest and lowest loaded aliskiren.

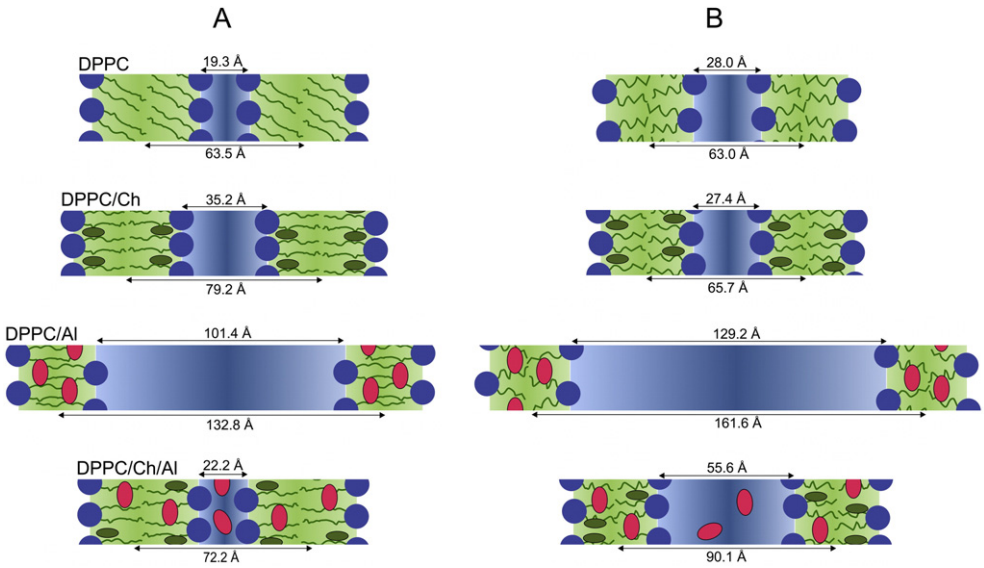

Fig. 9. Schematic representation of the pure DPPC, DPPC/cholesterol, DPPC/aliskiren and DPPC/cholesterol/aliskiren bilayers. For all four model membrane systems two adjacent bilayers are shown at 20 °C (A) and at 60 °C (B), respectively. Cholesterol molecules are coloured in green and aliskiren in red. Above each scheme the polar thickness (d-d_{HH}) and below the d-spacings are given. The data were derived from the SAXS data (see Section 3.4).

coefficient of aliskiren in the lamellar fluid phase would be in accordance with the given observations.

4.2. Location of aliskiren in the DPPC bilayers

Molecular dynamic simulations and NMR spectroscopy data have been used to locate the topography of the aliskiren in the lipid bilayers. The NMR data show almost no change in chemical shifts within the headgroup and glycerol backbone and only minor changes in the chemical shifts of the carbonyl region, when aliskiren is incorporated in DPPC bilayers. However; drastic changes appeared in the hydrophobic lipid chain region with its maximum at the carbon number 10. Thus, aliskiren is mainly centred around this carbon, both in the gel and liquid phases. Further, the MD simulations approve this finding (see the density profiles in Fig. 7B). We note, that Pomes and co-workers [61] pointed out that water-defect and lipid surface reorganization processes for small molecule may take as long as several microseconds. These long term processes are not included in our MD simulations, however, aliskiren places itself quite deep in the bilayer, where interfacial water-restructuring mechanism plays a minor role. Moreover, order parameter simulations demonstrate that aliskiren mainly accumulates at the centre of the hydrophobic lipid chain (Fig. 8B; corresponding to the carbon numbers 7 to 11 in the DPPC given in Fig. 1B).

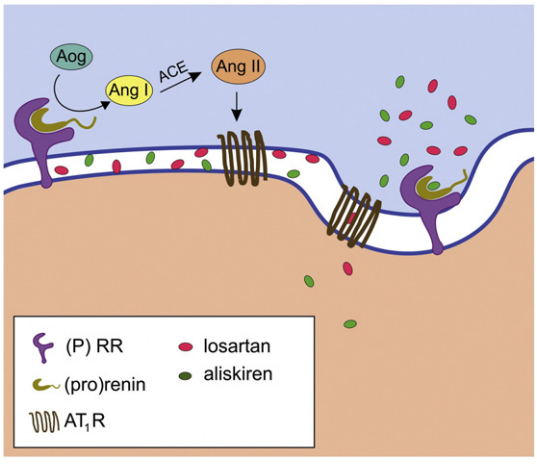

Fig. 10. Schematic representation of cholesterol-induced release of aliskiren and losartan. Left hand side: aliskiren and losartan accumulate in the lipid bilayer, but not necessarily inhibit the (P)RR and AT_1R. Angiotensinogen (Aog) gets cleaved by (P)RR-bound renin to angiotensin I (AngI), which by the angiotensin-converting enzyme (ACE) gets altered to the active peptide angiotensin II (AngII). Right hand side: as soon as a cholesterol rich caveolae is formed, aliskiren and losartan get released from the bilayer and block the receptors.

4.3. The influence of cholesterol

At 10 mol.% cholesterol content, both in the gel and the fluid phase regimes, cholesterol induces in part the liquid ordered (lo) phase causing a decrease of ΔH by 30% (Table 1). However, progressive addition of aliskiren into the DPPC/cholesterol composites increasingly diminishes the effect of cholesterol. Both aliskiren and AT_1R antagonist losartan act similarly against the lowering effect of ΔH caused by cholesterol [62].

Furthermore, cholesterol itself induces a condensing effect in the fluid lamellar phase of DPPC bilayers. This is observed in the increase of the Raman ratio at I_{1090}/I_{1130} by only about 15%. However, addition of cholesterol together with aliskiren causes a further increase of Raman ratio during the main phase transition ($\Delta I = 1.55 - 0.96 = 0.59$, Fig. 2A). The presence of aliskiren/cholesterol alike also causes significant increase in the I_{2850}/I_{2880} ratio meaning that the presence of these two components together causes disorder in the lipid bilayers (Fig. 2B). Thus, it can be understood that aliskiren causes fluidization of the lipid bilayers even in the presence of cholesterol. This is also confirmed by the bilayer thicknesses deduced from the SAXS data at 60 °C. The d_{HH} values for DPPC/aliskiren and DPPC/cholesterol/aliskiren do not differ significantly.

From the NMR data, it can be shown that cholesterol abolishes the pre-transition but, interestingly does not cause significant changes in the line-widths of the peaks (Fig. 3). This is an interesting observation and points out that, more complex motions are observed in DPPC/cholesterol bilayers as compared to DPPC/aliskiren or DPPC/cholesterol/aliskiren complexes.

While we have observed that aliskiren's incorporation induces a strong increase in the bilayer separations due to electrostatic repulsion, this effect is reduced under the presence of 10 mol.% cholesterol, i.e., we observe again a convergence of adjacent bilayers (see Fig. 9 bottom). A similar effect is apparent when losartan is interacting with DMPC/cholesterol membranes [15]. Initially, unbound membranes start to realign

in ordered stacks as the cholesterol content increases in the bilayer. Thus, it is tempting to assume that both losartan and also aliskiren get expelled from cholesterol rich membranes. This would at least deliver a straight forward explanation for the observed reduction in the bilayer separation distance.

In this respect, we briefly discuss a possible route of action of aliskiren. Due to its high lipophilicity [13] aliskiren is expected to accumulate as efficiently in lipid bilayers as the comprehensively studied ARBs [14–17] (Fig. 10, left hand side). However, when cholesterol rich domains (caveolae) would form in the direct vicinity of a (P)RR, then membrane-accumulated aliskiren molecules are likely to get expelled from the lipid bilayer due to the high concentration of cholesterol (cp. Fig. 4C and D), and the binding of the inhibitors to the active site becomes possible from the extracellular fluid (Fig. 10; right hand side). The same scenario could occur also for the mechanism of action of ARBs, i.e., also the AT_1R could be efficiently blocked by for instance membrane-bound losartans, when a cholesterol rich membrane caveolae is formed. This newly proposed mechanism is also interesting in the light of the increasingly investigated intracellular renin-angiotensin system [10,63].

5. Conclusion

The interactions of aliskiren with cholesterol-rich and cholesterol-poor plasma membrane models have been investigated both experimentally (DSC, Raman spectroscopy, NMR, X-ray scattering) and by MD simulations. It turned out that aliskiren behaves in many respects in a similar fashion as the beforehand studied ARBs. Aliskiren incorporates in the bilayer with a high affinity, but positions itself a bit deeper in the membrane core as compared to most of the ARBs. Similarly, aliskiren induces a partial interdigitation of the lipid chain in the gel phase. As a consequence, already at low concentrations the pretransition of DPPC gets suppressed. Moreover, the thermodynamic alterations (lowering of T_m and increasing of the main transition enthalpy) and fluidization effects on PC-model membranes have shown many parallels to the action of AT_1R antagonists. Most interestingly, already the presence of 10 mol.% cholesterol expels aliskiren at least in part from the membrane. This has led us to propose a refined mechanism of action of aliskiren for the case of its accumulation in the plasma membranes of e.g., vascular smooth muscle cells.

Acknowledgements

We kindly acknowledge Novartis for supplying us with aliskiren.

Appendix A. Supplementary data

Supplementary data to this article can be found online at http://dx.doi.org/10.1016/j.bbamem.2014.12.004.

References

[1] J.L. Zhuo, F.M. Ferrao, Y. Zheng, X.C. Li, New frontiers in the intrarenal renin-angiotensin system: a critical review of classical and new paradigms, Front. Endocrinol. 4 (2013) 166.
[2] J.L. Zhuo, X.C. Li, New insights and perspectives on intrarenal renin-angiotensin system: focus on intracrine/intracellular angiotensin II, Peptides 32 (2011) 1551–1565.
[3] T. Mavromoustakos, G. Agelis, S. Durdagi, AT1 antagonists: a patent review (2008–2012), Expert Opin. Ther. Patents 23 (2013) 1483–1494.
[4] P. Zoumpoulakis, I. Daliani, M. Zervou, I. Kyrikou, E. Siapi, G. Lamprinidis, E. Mikros, T. Mavromoustakos, Losartan's molecular basis of interaction with membranes and AT(1) receptor, Chem. Phys. Lipids 125 (2003) 13–25.
[5] M. Lucio, J.L.F.C. Lima, S. Reis, Drug-membrane interactions: significance for medicinal chemistry, Curr. Med. Chem. 17 (2010) 1795–1809.
[6] A.M. Seddon, D. Casey, R.V. Law, A. Gee, R.H. Templer, O. Ces, Drug interactions with lipid membranes, Chem. Soc. Rev. 38 (2009) 2509–2519.
[7] M. Zervou, Z. Cournia, C. Potamitis, G. Patargias, S. Durdagi, S.G. Grdadolnik, T. Mavromoustakos, Insights into the molecular basis of action of the AT(1) antagonist losartan using a combined NMR spectroscopy and computational approach, Biochim. Biophys. Acta Biomembr. 1838 (2014) 1031–1046.
[8] M. Azizi, R. Webb, J. Nussberger, N.K. Hollenberg, Renin inhibition with aliskiren: where are we now, and where are we going? J. Hypertens. 24 (2006) 243–256.
[9] W.W. Batenburg, A.H.J. Danser, (Pro)renin and its receptors: pathophysiological implications, Clin. Sci. 123 (2012) 121–133.
[10] R. Kumar, V.P. Singh, K.M. Baker, The intracellular renin-angiotensin system in the heart, Curr. Hypertens. Rep. 11 (2009) 104–110.
[11] G. Sihn, A. Rousselle, L. Vilianovitch, C. Burckle, M. Bader, Physiology of the (pro)renin receptor: Wnt of change? Kidney Int. 78 (2010) 246–256.
[12] G. Nguyen, F. Delarue, C. Burckle, L. Bouzhir, T. Giller, J.D. Sraer, Pivotal role of the renin/prorenin receptor in angiotensin II production and cellular responses to renin, J. Clin. Investig. 109 (2002) 1417–1427.
[13] J.M. Wood, J. Maibaum, J. Rahuel, M.G. Grutter, N.C. Cohen, V. Rasetti, H. Ruger, R. Goschke, S. Stutz, W. Fuhrer, W. Schilling, P. Rigollier, Y. Yamaguchi, F. Cumin, H.P. Baum, C.R. Schnell, P. Herold, R. Mah, C. Jensen, E. O'Brien, A. Stanton, M.P. Bedigian, Structure-based design of aliskiren, a novel orally effective renin inhibitor, Biochem. Biophys. Res. Commun. 308 (2003) 698–705.
[14] C. Fotakis, S. Gega, E. Siapi, C. Potamitis, K. Viras, P. Moutevelis-Minakakis, C.G. Kokotos, S. Durdagi, S. Golic Grdadolnik, B. Sartori, M. Rappolt, T. Mavromoustakos, Interactions at the bilayer interface and receptor site induced by the novel synthetic pyrrolidinone analog MMK3, Biochim. Biophys. Acta 1768 (2010) 422–432.
[15] A. Hodzic, P. Zoumpoulakis, G. Pabst, T. Mavromoustakos, M. Rappolt, Losartan's affinity to fluid bilayers modulates lipid–cholesterol interactions, Phys. Chem. Chem. Phys. 14 (2012) 4780–4788.
[16] D. Ntountaniotis, G. Mali, S.G. Grdadolnik, H. Maria, A.-L. Skaltsounis, C. Potamitis, E. Siapi, P. Chatzigeorgiou, M. Rappolt, T. Mavromoustakos, Thermal, dynamic and structural properties of drug AT(1) antagonist olmesartan in lipid bilayers, Biochim. Biophys. Acta Biomembr. 1808 (2011) 2995–3006.
[17] C. Potamitis, P. Chatzigeorgiou, E. Siapi, K. Viras, T. Mavromoustakos, A. Hodzic, G. Pabst, F. Cacho-Nerin, P. Laggner, M. Rappolt, Interactions of the AT(1) antagonist valsartan with dipalmitoyl-phosphatidylcholine bilayers, Biochim. Biophys. Acta Biomembr. 1808 (2011) 1753–1763.
[18] T.R. Oliveira, M.T. Lamy, U.M. De Paula, L.L. Guimar+úes, M.S. Toledo, H.K. Takahashi, A.H. Straus, C.J. Lindsey, T.B. Paiva, Structural properties of lipid reconstructs and lipid composition of normotensive and hypertensive rat vascular smooth muscle cell membranes, Braz. J. Med. Biol. Res. 42 (2009) 844–853.
[19] T.J. Netticadan, T.F. Ashavaid, K.G. Nair, Characterisation of the canine cardiac sarcolemma in experimental myocardial ischemia, Indian J. Clin. Biochem. : IJCB 12 (1997) 49–54.
[20] R. Koynova, M. Caffrey, Phases and phase transitions of the phosphatidylcholines, Biochim. Biophys. Acta Rev. Biomembr. 1376 (1998) 91–145.
[21] B. Pilz, E. Shagdarsuren, M. Wellner, A. Fiebeler, R. Dechend, P. Gratze, S. Meiners, D.L. Feldman, R.L. Webb, I.M. Garrelds, A.H.J. Danser, F.C. Luft, D.N. Muller, Aliskiren, a human renin inhibitor, ameliorates cardiac and renal damage in double-transgenic rats, Hypertension 46 (2005) 569–576.
[22] Y. Zhang, Y. Wang, Y. Chen, D.K. Deb, T. Sun, Q. Zhao, Y.C. Li, Inhibition of renin activity by aliskiren ameliorates diabetic nephropathy in type 1 diabetes mouse model, J. Diabetes Mellitus 2 (2012) 353–360.
[23] G. Metz, X.L. Wu, S.O. Smith, Ramped amplidtude cross-polarization in magic-angle-spinning NMR, J. Magn. Reson. Ser. A 110 (1994) 219–227.
[24] H. Amenitsch, M. Rappolt, M. Kriechbaum, H. Mio, P. Laggner, S. Bernstorff, First performance assessment of the small-angle X-ray scattering beamline at ELETTRA, J. Synchrotron Radiat. 5 (1998) 506–508.
[25] S. Bernstorff, H. Amenitsch, P. Laggner, High-throughput asymmetric double-crystal monochromator of the SAXS beamline at ELETTRA, J. Synchrotron Radiat. 5 (1998) 1215–1221.
[26] M. Rappolt, A. Hodzic, B. Sartori, M. Ollivon, P. Laggner, Conformational and hydrational properties during the L(beta)- to L(alpha)- and L alpha- to H(II)-phase transition in phosphatidylethanolamine, Chem. Phys. Lipids 154 (2008) 46–55.
[27] M. Rappolt, The biologically relevant lipid mesophases as "seen" by X-rays, Adv. Planar Lipid Bilayers Liposomes 5 (5) (2007) 253–283.
[28] A. Caillé, Remarques sur la diffusion des rayons X dans les smectiques A, C. R. Acad. Sci. Paris B 274 (1972) 891–893.
[29] R. Zhang, R.M. Suter, J.F. Nagle, Theory of the structure factor of lipid bilayers, Phys. Rev. E. 50 (1994) 5047–5060.
[30] P.G. De Gennes, J. Prost, The Physics of Liquid Crystals, 2nd edition Oxford University Press, Oxford, 1993.
[31] G. Pabst, M. Rappolt, H. Amenitsch, P. Laggner, Structural information from multilamellar liposomes at full hydration: full q-range fitting with high quality x-ray data, Phys. Rev. E. 62 (2000) 4000–4009.
[32] G. Pabst, J. Katsaras, V.A. Raghunathan, M. Rappolt, Structure and interactions in the anomalous swelling regime of phospholipid bilayers, Langmuir 19 (2003) 1716–1722.
[33] M. Rappolt, G. Pabst, Flexibility and structure of fluid bilayer interfaces, in: K. Nag (Ed.), Structure and Dynamics of Membranous Interfaces, John Wiley & Sons, Hoboken, 2008, pp. 45–81.
[34] M. Rappolt, Bilayer thickness estimations with "poor" diffraction data, J. Appl. Phys. 107 (2010) (084701–084701–084701–084707).
[35] S. Baoukina, D.P. Tieleman, Simulations of Lipid Monolayers, in: L. Monticelli, E. Salonen (Eds.), Biomolecular Simulations, vol. 924, Humana Press, 2013, pp. 431–444.
[36] D.P. Tieleman, H.J.C. Berendsen, Molecular dynamics simulations of a fully hydrated dipalmitoyl phosphatidylcholine bilayer with different macroscopic boundary conditions and parameters, J. Chem. Phys. 105 (1996) 4871–4880.
[37] O. Berger, O. Edholm, F. Jahnig, Molecular dynamics simulations of a fluid bilayer of dipalmitoylphosphatidylcholine at full hydration, constant pressure, and constant temperature, Biophys. J. 72 (1997) 2002–2013.
[38] D. Van der Spoel, E. Lindahl, B. Hess, G. Groenhof, A.E. Mark, H.J.C. Berendsen, GROMACS: fast, flexible, and free, J. Comput. Chem. 26 (2005) 1701–1718.

[39] B. Hess, C. Kutzner, D. van der Spoel, E. Lindahl, GROMACS 4: algorithms for highly efficient, load-balanced, and scalable molecular simulation, J. Chem. Theory Comput. 4 (2008) 435–447.
[40] D. van der Spoel, E. Lindahl, B. Hess, A.R. van Buuren, E. Apol, P.J. Meulenhoff, A. Sijbers, K.A. Feenstra, R. van Drumen, H.J.C. Berendsen, GROMACS user manual, Nijenborgh 4 (2010).
[41] M.H.F. Wilkins, A.E. Blaurock, D.M. Engelman, Bilayer structure in membranes, Nat. New Biol. 230 (1971) 72-&.
[42] W.J. Sun, S. TristramNagle, R.M. Suter, J.F. Nagle, Structure of the ripple phase in lecithin bilayers, Proc. Natl. Acad. Sci. U. S. A. 93 (1996) 7008–7012.
[43] J.F. Nagle, S. Tristram-Nagle, Structure of lipid bilayers, Biochim. Biophys. Acta Rev. Biomembr. 1469 (2000) 159–195.
[44] N. Yellin, I.W. Levin, Hydrocarbon chain trans–gauche isomerization in phospholipid bilayer gel assemblies, Biochemistry 16 (1977) 642–647.
[45] N. Yellin, I.W. Levin, Hydrocarbon chain disorder in lipid bilayers: temperature dependent Raman spectra of 1,2-diacylphosphatidylcholine-water gels, Biochim. Biophys. Acta 489 (1977) 177–190.
[46] R.C. Spiker, I.W. Levin, Raman spectra and vibrational assignments for dipalmotylphosphatidylcholine and structurally related molecules, Biochim. Biophys. Acta 388 (1975) 361–373.
[47] N.B. Colthulp, L.H. Daly, S.E. Wiberley, Introduction to Infrared and Raman Spectroscopy, Academic Press, 1990.
[48] A. Ramamoorthy, Beyond NMR spectra of antimicrobial peptides: dynamical images at atomic resolution and functional insights, Solid State Nucl. Magn. Reson. 35 (2009) 201–207.
[49] M. Rappolt, P. Laggner, G. Pabst, Structure and elasticity of phospholipid bilayers in the Lα phase: a comparison of phosphatidylcholine and phosphatidylethanolamine membranes, in: S.G. Pandalai (Ed.)Recent Research Developments in Biophysics, Part II, Transworld Research Network, Trivandrum, vol. 3, 2004, pp. 365–394.
[50] S. Tristramnagle, R. Zhang, R.M. Suter, C.R. Worthington, W.J. Sun, J.F. Nagle, Measurement of chain tilt angle in fully hydrated bilayers of gel phase lecithins, Biophys. J. 64 (1993) 1097–1109.
[51] M. Rappolt, G. Rapp, Structure of the stable and metastable ripple phase of dipalmitoylphosphatidylcholine, Eur. Biophys. J. Biophys. Lett. 24 (1996) 381–386.
[52] M.R. Vist, J.H. Davis, Phase equilibria of cholesterol/dipalmitoylphosphatidylcholine mixtures: 2H nuclear magnetic resonance and differential scanning calorimetry, Biochemistry 29 (1990) 451–464.
[53] M. Rappolt, M.F. Vidal, M. Kriechbaum, M. Steinhart, H. Amenitsch, S. Bernstorff, P. Laggner, Structural, dynamic and mechanical properties of POPC at low cholesterol concentration studied in pressure/temperature space, Eur. Biophys. J. Biophys. Lett. 31 (2003) 575–585.
[54] A. Hodzic, M. Rappolt, H. Amenitsch, P. Laggner, G. Pabst, Differential modulation of membrane structure and fluctuations by plant sterols and cholesterol, Biophys. J. 94 (2008) 3935–3944.
[55] A. Seelig, J. Seelig, The dynamic structure of fatty acyl chains in a phospholipid bilayer measured by deuterium magnetic resonance, Biochemistry 13 (1974) 4839–4845.
[56] R.G. Griffin, Solid state nuclear magnetic resonance of lipid bilayers, Methods Enzymol. 72 (1981) 108–174.
[57] C. Fotakis, D. Christodoueas, P. Zoumpoulakis, E. Kritsi, N.-P. Benetis, T. Mayromoustakos, H. Reis, A. Gili, M.G. Papadopoulos, M. Zervou, Comparative biophysical studies of sartan class drug molecules losartan and candesartan (CV-11974) with membrane bilayers, J. Phys. Chem. B 115 (2011) 6180–6192.
[58] I.W. Levin, E.N. Lewis, Fourier transform Raman spectroscopy of biological materials, Anal. Chem. 62 (1990) 1101A.
[59] R.K. Bista, R.F. Bruch, A.M. Covington, Variable-temperature Raman spectromicroscopy for a comprehensive analysis of the conformational order in PEGylated lipids, J. Raman Spectrosc. 40 (2009) 463–471.
[60] I.F. Alexa, M. Ignat, R.F. Popovici, D. Timpu, E. Popovici, In vitro controlled release of antihypertensive drugs intercalated into unmodified SBA-15 and MgO modified SBA-15 matrices, Int. J. Pharm. 436 (2012) 111–119.
[61] C. Neale, W.F.D. Bennett, D.P. Tieleman, R. Pomes, Statistical convergence of equilibrium properties in simulations of molecular solutes embedded in lipid bilayers, J. Chem. Theory Comput. 7 (2011) 4175–4188.
[62] T. Mavromoustakos, P. Chatzigeorgiou, C. Koukoulitsa, S. Durdagi, Partial interdigitation of lipid bilayers, Int. J. Quantum Chem. 111 (2011) 1172–1183.
[63] G. Jagadeesh, P. Balakumar, N. Stockbridge, How well do aliskiren's purported mechanisms track its effects on cardiovascular and renal disorders? Cell. Signal. 24 (2012) 1583–1591.